

Orthogonalized Policy Optimization

Decoupling Sampling Geometry from Optimization Geometry in RLHF

Wang Zixian

China Mobile Communications Group Shandong Co., Ltd. Tai'an Branch

wangzixian@sd.chinamobile.com

Abstract

We present **Orthogonalized Policy Optimization (OPO)**, a unified theoretical account of LLM alignment grounded in a *work-dissipation principle*. The policy update is characterized as a constrained proximal response that maximizes external work induced by an α -escort sampling field, while paying an intrinsic dissipation cost given by a quadratic fluctuation energy in χ^2 (ratio) geometry. This single variational principle simultaneously admits three equivalent interpretations: (i) a *mirror-descent* step with a Euclidean mirror map in ratio space, (ii) a *Hilbert-space projection* via the orthogonal projection theorem in $L^2(\pi_k)$, and (iii) a *linear-response* law from near-equilibrium statistical mechanics. Their convergence to the same closed-form update confirms that OPO is the unique quadratic proximal response within ratio geometry. The framework cleanly decouples sampling geometry (α) from optimization geometry (μ), yields constant Hessian and non-saturating linear gradients, and reveals that advantage z -score normalization is not a heuristic but a conservation-law projection. Experiments on mathematical reasoning tasks demonstrate that OPO outperforms GRPO, GSPO, and DAPO while maintaining healthy gradient dynamics throughout training.

1 Introduction

Aligning Large Language Models (LLMs) with human preferences has become a cornerstone of modern AI development. The standard paradigm, Reinforcement Learning from Human Feedback (RLHF) [5, 6], typically employs algorithms like Proximal Policy Optimization (PPO) [2] or Direct Preference Optimization (DPO) [1] to optimize a policy against a reward model or preference dataset. Despite their formulation differences, these methods share a common structural foundation: they all rely on Kullback–Leibler (KL) divergence to constrain the policy update, preventing it from deviating excessively from a reference distribution.

While empirically effective, KL-regularized objectives exhibit distinct limitations in reasoning-intensive domains where high confidence is required. As the policy improves and assigns high probability to correct reasoning chains, the KL penalty—which induces an exponential geometry in the log-probability space—often dominates the learning signal. This manifests as gradient saturation, where the driving force for further improvement vanishes exponentially as the model becomes confident. Consequently, training often plateaus prematurely, behavior commonly attributed to “over-regularization” but which we argue is intrinsic to the chosen geometry.

We contend that this issue stems from a structural conflation in existing objective designs. Fundamentally, alignment involves two independent design choices: *sampling geometry*, which determines the effective weighting of training examples (e.g., whether to focus on high-advantage samples), and *optimization geometry*, which determines the curvature of the update step (e.g., how to measure distance in the policy space). In standard KL-based methods, a single divergence term dictates both, coupling the exploration strength with the optimization stability. Adjusting one inevitably perturbs the other, creating a dilemma where aggressive sampling destabilizes training, while stable optimization stifles exploration.

To resolve this, we propose a unifying framework based on a **work-dissipation principle**: the policy update maximizes *external work* induced by an α -escort sampling field, while paying an *intrinsic dissipation cost* in χ^2 ratio geometry. This single variational principle cleanly decouples the two axes

and admits three equivalent mathematical interpretations—mirror descent, Hilbert-space projection, and linear response—each illuminating a different structural facet.

Our contributions are as follows:

- We identify the implicit coupling of sampling and optimization geometries in KL-based alignment methods as a root cause of gradient saturation.
- We propose a unified *work–dissipation principle* that decouples these design axes: α -escort shapes the driving force, while a χ^2 quadratic penalty shapes the optimization curvature.
- We show that the resulting OPO objective admits three equivalent interpretations—Bregman mirror descent, Hilbert-space orthogonal projection, and near-equilibrium linear response—confirming it is the unique quadratic proximal response in ratio geometry. The Hilbert derivation further reveals that advantage z -score normalization is a conservation-law projection.
- We empirically demonstrate that OPO outperforms strong baselines (GRPO, GSPO, DAPO) on mathematical reasoning tasks. A *gradient response efficiency* analysis—normalizing gradient magnitude by the advantage signal amplitude—reveals that OPO maintains $\sim 5\times$ higher gradient-per-signal than KL-based baselines, providing direct quantitative evidence for the linear response prediction.

2 Related Work

Preference Optimization and RLHF. Reinforcement Learning from Human Feedback (RLHF) typically involves learning a reward model from preferences and then optimizing a policy via PPO [2, 5, 6]. Direct Preference Optimization (DPO) [1] simplifies this by deriving a closed-form solution to the KL-constrained reward maximization problem. Recent variants extend this paradigm: IPO [7] adds a regularization term to prevent overfitting, SimPO [8] simplifies the reference-free objective.

f -Divergences in Machine Learning. The f -divergence family [9, 10] provides a unified framework for measuring distributional discrepancy. The Csiszár–Amari α -divergence [9, 11] continuously connects forward and reverse KL. Prior work has explored f -divergences in variational inference [12], GANs [13], and imitation learning [14]. In RL, α PPO [15] studied α -divergence as a trust-region constraint. Recently, APO [16] explored combining forward and reverse KL dynamics for standard preference optimization. OPO builds on these foundations by decomposing the divergence into independent geometry axes.

Trust-Region Methods. TRPO [3] enforces stability via explicit KL constraints, while PPO [2] approximates this with ratio clipping. ADPO [17] shows that anchored coordinates provide an implicit trust region via temperature-scaled curvature. OPO extends this by replacing the KL-based geometry with a quadratic (χ^2) geometry in ratio coordinates, providing a different form of implicit regularization.

3 Preliminaries: Ratio Coordinates and Conservation

Let π_k denote the anchor (reference) policy at iteration k , with $\pi_k(y) > 0$ on its support.

Definition 3.1 (Ratio and Log-Ratio Coordinates). Define

$$t(y) := \frac{\pi(y)}{\pi_k(y)}, \quad v(y) := t(y) - 1 = \frac{\pi(y)}{\pi_k(y)} - 1, \quad \Delta(y) := \log \pi(y) - \log \pi_k(y). \quad (1)$$

Then $t(y) = e^{\Delta(y)}$ and $v(y) = e^{\Delta(y)} - 1$.

Conservation law. Probability normalization $\sum_y \pi(y) = 1$ is equivalent to

$$\mathbb{E}_{\pi_k}[t] = 1 \iff \mathbb{E}_{\pi_k}[v] = 0. \quad (2)$$

Hence admissible fluctuations lie in the closed subspace

$$\mathcal{H}_0 := \{v \in L^2(\pi_k) : \mathbb{E}_{\pi_k}[v] = 0\}. \quad (3)$$

4 Unified Work–Dissipation Principle

This section provides the unifying core: OPO is a constrained proximal response that maximizes *external work* induced by sampling geometry, while paying an *intrinsic dissipation* (fluctuation) energy that stabilizes the update.

4.1 Sampling Geometry as an α -Escort Field

Let P^* be an oracle target distribution encoding preference/quality. A canonical choice is $P^*(y) \propto \exp(A(y))$ where A is an advantage-like signal.

Definition 4.1 (α -Escort Distribution and Escort Weight). For $\alpha \in [0, 1]$, define the escort distribution

$$\rho_\alpha(y) \propto \pi_k(y)^\alpha P^*(y)^{1-\alpha}. \quad (4)$$

Define the escort weight (Radon–Nikodym derivative)

$$\omega_\alpha(y) := \frac{\rho_\alpha(y)}{\pi_k(y)}. \quad (5)$$

Since ρ_α is normalized,

$$\mathbb{E}_{\pi_k}[\omega_\alpha] = 1. \quad (6)$$

Proposition 4.2 (α -Geometric Interpolation). *The family $\{\rho_\alpha\}_{\alpha \in [0,1]}$ forms an e -geodesic connecting P^* (at $\alpha = 0$) to π_k (at $\alpha = 1$). The escort weight simplifies to $\omega_\alpha(y) \propto (\exp(A(y))/\pi_k(y))^{1-\alpha}$.*

Geometric semantics. α controls how aggressively sampling emphasizes high-quality regions: $\alpha \rightarrow 1$ gives $\omega_\alpha \rightarrow 1$ (conservative); $\alpha \rightarrow 0$ gives $\omega_\alpha \rightarrow P^*/\pi_k$ (aggressive).

On-policy implementation (stop-gradient). When $\pi_k = \pi_{\text{old}}$ is frozen during an iteration,

$$\omega_\alpha(y) \propto \exp((1-\alpha)A(y)) \cdot \text{sg}\left(\pi_k(y)^{-(1-\alpha)}\right). \quad (7)$$

Batch normalization of escort weights. The escort density $\rho_\alpha(y) \propto \pi_k(y)^\alpha P^*(y)^{1-\alpha}$ involves an unknown normalizing constant Z_α . In practice we do not compute Z_α explicitly; instead, we apply batch-wise zero-centering and z -scoring of ω_α over each mini-batch. This is equivalent to estimating the normalizer locally within the sample batch, and ensures that the estimated weights satisfy the mean constraint $\mathbb{E}[\omega_\alpha] = 1$ at the sample level. The subsequent mean subtraction in the OPO update (Remark 6.2) absorbs any residual bias.

4.2 Intrinsic Dissipation Energy as Quadratic Fluctuation Cost

We stabilize the update by penalizing the fluctuation amplitude $v = \pi/\pi_k - 1$ in $L^2(\pi_k)$:

$$\mathcal{E}_{\text{diss}}(v) := \frac{\mu}{2} \|v\|_{L^2(\pi_k)}^2 = \frac{\mu}{2} \mathbb{E}_{\pi_k}[v(y)^2]. \quad (8)$$

This is exactly the Pearson χ^2 geometry in ratio coordinates: $\mathbb{E}_{\pi_k}[v^2] = \mathbb{E}_{\pi_k}[(\pi/\pi_k - 1)^2]$.

Physical motivation. Near the anchor, a quadratic fluctuation cost matches the universal Gaussian-fluctuation principle from near-equilibrium thermodynamics: small departures from equilibrium incur a quadratic free-energy cost [19].

4.3 OPO as a Constrained Work–Dissipation Balance

Define the work–dissipation functional

$$v^* = \arg \max_{v \in L^2(\pi_k)} \left\{ \underbrace{\langle \omega_\alpha, v \rangle}_{\text{external work}} - \underbrace{\frac{\mu}{2} \|v\|^2}_{\text{intrinsic dissipation}} \right\} \quad \text{s.t.} \quad \mathbb{E}_{\pi_k}[v] = 0. \quad (9)$$

Equivalently, in loss-minimization form,

$$\boxed{\mathcal{L}_{\text{OPO}}(v) = -\mathbb{E}_{\pi_k}[\omega_\alpha(y) v(y)] + \frac{\mu}{2} \mathbb{E}_{\pi_k}[v(y)^2], \quad \mathbb{E}_{\pi_k}[v] = 0.} \quad (10)$$

Orthogonality of the two geometries. α enters only through ω_α (first-order drive); μ enters only through the quadratic curvature (second-order geometry). Sampling and optimization are *structurally orthogonal*.

4.4 Closed-Form Solution (Linear Response Law)

Theorem 4.3 (Closed-Form Update). *The unique optimizer of Eq. (9) is*

$$\boxed{v^*(y) = \frac{1}{\mu} (\omega_\alpha(y) - 1).} \quad (11)$$

Proof. Introduce a Lagrange multiplier λ for $\mathbb{E}_{\pi_k}[v] = 0$. Stationarity gives $0 = -\omega_\alpha(y) + \mu v(y) + \lambda$. Taking $\mathbb{E}_{\pi_k}[\cdot]$ and using $\mathbb{E}_{\pi_k}[v] = 0$ yields $\lambda = \mathbb{E}_{\pi_k}[\omega_\alpha] = 1$. Substituting back gives $v^* = (\omega_\alpha - 1)/\mu$.

Policy update. Since $\pi = \pi_k(1 + v)$,

$$\frac{\pi_{k+1}(y)}{\pi_k(y)} = 1 + \frac{1}{\mu} (\omega_\alpha(y) - 1). \quad (12)$$

Non-saturating linear dynamics. The function-space gradient is $\nabla_v \mathcal{L}_{\text{OPO}} = -\omega_\alpha + \mu v$, which is linear in v with constant curvature $\nabla_v^2 \mathcal{L} = \mu I$. Unlike sigmoid/logistic objectives, this does not exhibit exponential saturation.

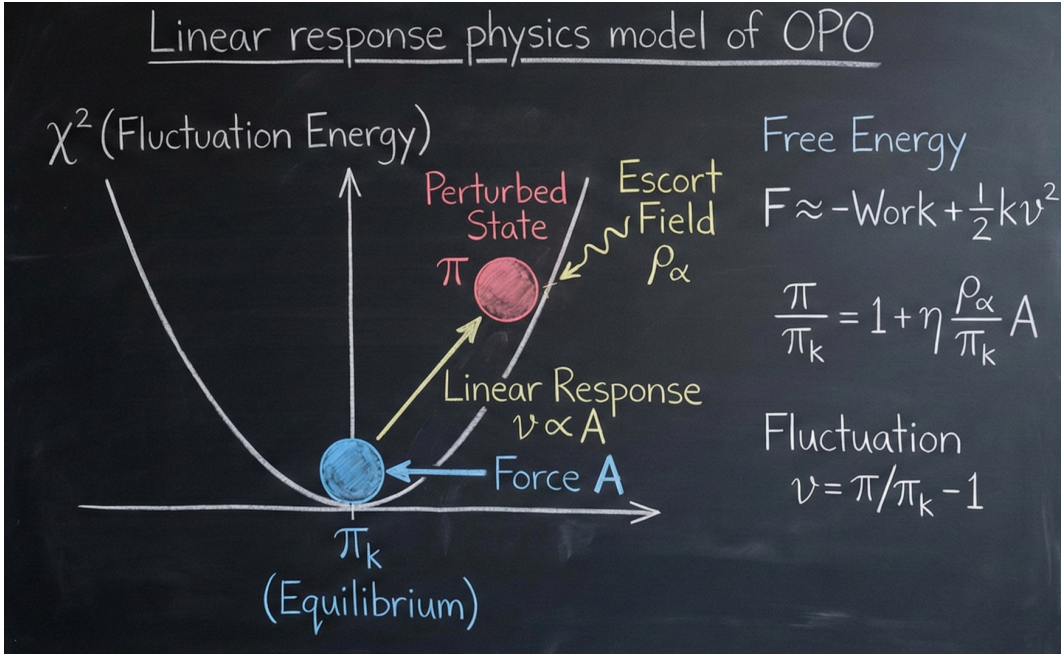


Figure 1: Work–dissipation physics picture of OPO. The anchor policy π_k sits at the minimum of a quadratic fluctuation energy (χ^2 geometry). The escort field ρ_α induces the driving weight $\omega_\alpha = \rho_\alpha/\pi_k$. The perturbed policy π corresponds to a ratio fluctuation $v = \pi/\pi_k - 1$. The conservation law $\mathbb{E}_{\pi_k}[v] = 0$ forces an orthogonal projection, yielding the centered response $v^* = (\omega_\alpha - 1)/\mu$. In statistical mechanics [18], this is the *fluctuation–dissipation theorem*: response equals susceptibility ($1/\mu$) times centered driving force.

5 Mirror Descent Interpretation

We show that the work–dissipation principle is equivalently a mirror descent step with a Euclidean mirror map.

5.1 Euclidean Mirror Map and χ^2 Bregman Divergence

Define the mirror map $\Psi(v) := \frac{1}{2}\|v\|_{L^2(\pi_k)}^2$. The induced Bregman divergence is

$$D_\Psi(\pi\|\pi_k) = \frac{1}{2}\mathbb{E}_{\pi_k}\left[\left(\frac{\pi}{\pi_k} - 1\right)^2\right], \quad (13)$$

which is the Pearson χ^2 divergence in ratio coordinates.

5.2 Orthogonal Mirror Step

A mirror/proximal step driven by ω_α is

$$v^* = \arg \min_{v \in \mathcal{H}_0} \left\{ -\langle \omega_\alpha, v \rangle + \frac{\mu}{2}\|v\|^2 \right\}, \quad (14)$$

which is identical to the work–dissipation formulation (9). Thus mirror descent and the free-energy principle define the *same* update. α affects only the drive ω_α ; μ affects only the proximal curvature.

6 Hilbert Projection Interpretation

We re-derive the same objective from the Hilbert space projection theorem, requiring no mirror maps.

6.1 Hilbert Space and Metric Modulation

Let $\mathcal{H} = L^2(\pi_k)$ with inner product $\langle f, g \rangle = \mathbb{E}_{\pi_k}[fg]$. Define the multiplication operator (diagonal preconditioner)

$$(\mathcal{M}_\alpha f)(y) := \omega_\alpha(y) f(y). \quad (15)$$

Lemma 6.1 (Boundedness, Self-Adjointness, Positivity). *If $\omega_\alpha \in L^\infty(\pi_k)$ and $\omega_\alpha > 0$ a.s., then \mathcal{M}_α is bounded, self-adjoint, and positive. The induced inner product $\langle f, g \rangle_\alpha := \mathbb{E}_{\rho_\alpha}[fg]$ is the escort-modulated geometry.*

Thus α -escort is a smooth *metric modulation*: it preserves support and reweights directions in function space through a new local inner product, in contrast to hard masking which truncates support.

6.2 Projection Theorem Gives the Same Closed Form

Rewrite Eq. (9) by completing the square:

$$\langle \omega_\alpha, v \rangle - \frac{\mu}{2} \|v\|^2 = -\frac{\mu}{2} \left\| v - \frac{1}{\mu} \omega_\alpha \right\|^2 + \frac{1}{2\mu} \|\omega_\alpha\|^2. \quad (16)$$

Hence

$$v^* = \arg \min_{v \in \mathcal{H}_0} \left\| v - \frac{1}{\mu} \omega_\alpha \right\|^2. \quad (17)$$

By the Hilbert projection theorem,

$$v^* = \frac{1}{\mu} \mathcal{P}_{\mathcal{H}_0}(\omega_\alpha) = \frac{1}{\mu} (\omega_\alpha - \langle \omega_\alpha, 1 \rangle 1) = \frac{1}{\mu} (\omega_\alpha - 1), \quad (18)$$

recovering Theorem 4.3. The subtraction of 1 is the unique orthogonal correction enforced by conservation.

Remark 6.2 (z -Score Normalization as Conservation-Law Projection). The centering $\omega_\alpha \mapsto \omega_\alpha - \mathbb{E}[\omega_\alpha]$ is exactly $\mathcal{P}_{\mathcal{H}_0}$ —the mean-subtraction step of z -score normalization. When $\omega_\alpha(y) = A(y)$ ($\alpha \rightarrow 1$), the solution $v^* = (A - \mathbb{E}[A])/\mu$ is the z -scored advantage scaled by susceptibility. Thus, advantage z -scoring is not a variance-reduction heuristic: it is the *unique orthogonal projection* enforcing probability conservation in $L^2(\pi_k)$.

Remark 6.3 (Contrast with Fisher–Rao (KL) Geometry). In KL-based methods, the natural metric is the Fisher–Rao metric $g_{ij}^{\text{FR}} = \mathbb{E}_\pi[\partial_i \log \pi \cdot \partial_j \log \pi]$, whose curvature depends on π . In contrast, χ^2 geometry operates in $L^2(\pi_k)$ with *constant* inner product:

	KL / Fisher–Rao	$\chi^2 / L^2(\pi_k)$
Inner product	Fisher metric (policy-dependent)	$L^2(\pi_k)$ (fixed at anchor)
Hessian	$\nabla^2 \propto \beta^2 \sigma(1-\sigma)$	$\nabla^2 = \mu I$ (constant)
Perturbation theory	Nonlinear (exponential)	Linear (first-order exact)

7 Implementable Surrogate and Algorithm

7.1 Log-Ratio Surrogate for LLMs

LLMs output log-probabilities. Let $\Delta_\theta(y) := \log \pi_\theta(y) - \log \pi_k(y)$. Since $v = e^\Delta - 1 \approx \Delta$ for small trust regions, the practical surrogate is

$$\mathcal{L}_{\text{OPO}}^{\log}(\theta) = -\mathbb{E}_{\pi_k} [\omega_\alpha(y) \Delta_\theta(y)] + \frac{\mu}{2} \mathbb{E}_{\pi_k} [\Delta_\theta(y)^2]. \quad (19)$$

Anchoring $\pi_k = \pi_{\text{old}}$ resets Δ near zero each iteration, supporting the local approximation.

7.2 Algorithm and Flowchart

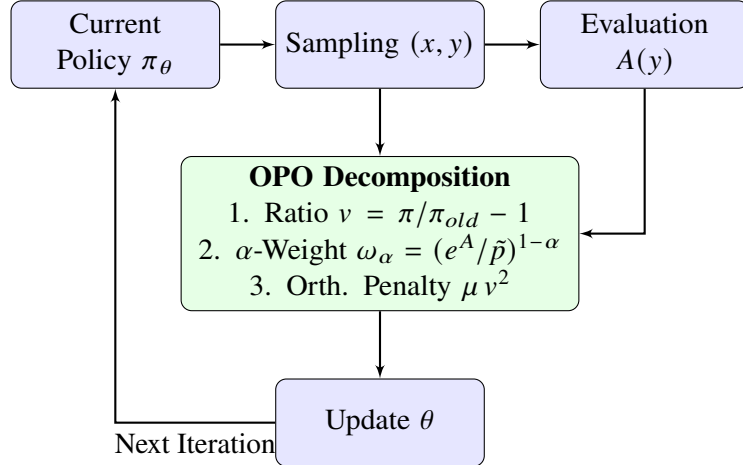


Figure 2: Flowchart of the OPO framework. The “OPO Decomposition” block (green) embodies the work–dissipation structure: the α -escort (step 2) shapes the external work, while the χ^2 penalty (step 3) shapes the intrinsic dissipation. The two axes are structurally orthogonal.

Algorithm 1 Orthogonalized Policy Optimization (OPO)

Require: Initial policy π_θ ; parameters $\alpha \in [0, 1]$, $\mu > 0$, $\eta > 0$

- 1: **for** each iteration **do**
- 2: **Anchor:** $\pi_{\text{ref}} \leftarrow \pi_\theta$ ▷ On-policy anchoring
- 3: **Rollout:** Sample $(x, y) \sim \pi_\theta$; compute rewards $R(x, y)$
- 4: **Advantage:** $A(y) \leftarrow \text{zscore}(R(x, y))$ ▷ Group z -score (Remark 6.2)
- 5: **Escort Weight:** $\omega_\alpha(y) \leftarrow \exp((1-\alpha) A(y)) \cdot \text{sg}(\pi_{\text{ref}}(y)^{-(1-\alpha)})$ ▷ Eq. 7
- 6: **Log-Ratio:** $\Delta_\theta(y) \leftarrow \log \pi_\theta(y) - \log \pi_{\text{ref}}(y)$
- 7: **Loss:** $\mathcal{L} \leftarrow \frac{1}{N} \sum_y \left[-\omega_\alpha(y) \Delta_\theta(y) + \frac{\mu}{2} \Delta_\theta(y)^2 \right]$
- 8: **Update:** $\theta \leftarrow \theta - \eta \nabla_\theta \mathcal{L}$
- 9: **end for**

8 Theoretical Analysis

8.1 Constant Curvature and Orthogonal Control

Theorem 8.1 (Decoupling of Sampling and Optimization Geometry). *Consider the OPO objective in v -space. Then:*

1. *The first-order drive depends on α only through ω_α : $\nabla_v \mathcal{L}_{\text{OPO}} = -\omega_\alpha + \mu v$.*
2. *The second-order curvature is constant and independent of α : $\nabla_v^2 \mathcal{L}_{\text{OPO}} = \mu I$.*

Changing α reshapes the target (what to learn) without altering curvature (how to learn). Changing μ alters curvature without reshaping the target.

8.2 Global Contraction in v -Space

Gradient descent $v^{(m+1)} = v^{(m)} - \eta(\mu v^{(m)} - \omega_\alpha)$ satisfies

$$v^{(m+1)} - v^* = (1 - \eta\mu)(v^{(m)} - v^*). \quad (20)$$

Corollary 8.2 (Linear Rate). *For $0 < \eta < 2/\mu$, $\|v^{(m)} - v^*\| \leq |1 - \eta\mu|^m \|v^{(0)} - v^*\|$. The contraction rate depends only on μ and is independent of α .*

8.3 Why KL-Based Objectives Saturate

In KL-regularized preference optimization, local curvature scales like $\sigma(m)(1 - \sigma(m))$ and vanishes exponentially as $|m| \rightarrow \infty$. By contrast, OPO has constant curvature μI and linear restoring force $\|\nabla_v \mathcal{L}\| = \|\mu(v - v^*)\|$, which remains proportional to distance-to-equilibrium.

Figure 3 visualizes this contrast on a binary logit toy model ($z_{\text{ref}} = 0$). Panel (a) plots $|\partial \mathcal{L} / \partial z|$ versus the model confidence $p = \sigma(z)$: SFT, DPO, GRPO, DAPO, and GSPO all decay to zero in the high-confidence regime, while OPO's χ^2 gradient grows linearly. Panel (b) zooms into $p \geq 0.5$ on a logarithmic scale, revealing that clipped objectives (GRPO, DAPO, GSPO) suffer a hard cliff to machine-epsilon once the ratio exits the clip window, and DPO saturates exponentially. OPO is the only objective whose gradient magnitude remains $O(1)$ throughout.

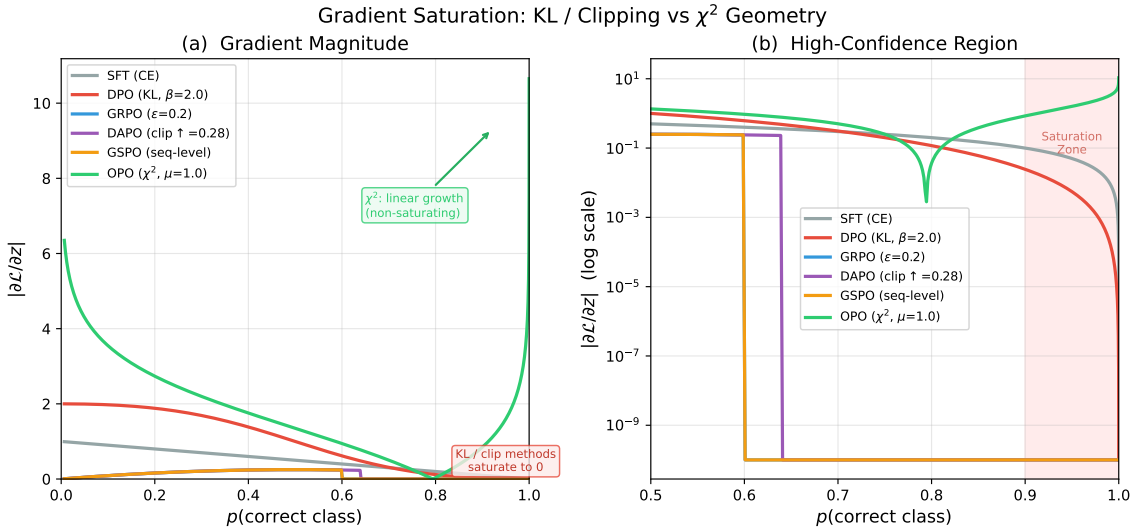


Figure 3: Toy gradient saturation experiment (binary logit, $z_{\text{ref}} = 0$). (a) Gradient magnitude vs. model confidence: OPO (χ^2 , green) exhibits linear growth while all other objectives saturate. (b) Log-scale zoom on $p \geq 0.5$: clipped objectives cliff-drop by up to 9 orders of magnitude; OPO maintains non-vanishing gradients throughout.

8.4 Trust-Region Duality

Proposition 8.3 (χ^2 Trust-Region Duality). *The constrained problem $\max_{v \in \mathcal{H}_0} \langle \omega_\alpha, v \rangle$ s.t. $\|v\|^2 \leq \varepsilon$ has Lagrangian relaxation $\max_{v \in \mathcal{H}_0} \langle \omega_\alpha, v \rangle - \frac{\mu}{2} \|v\|^2$, with μ as the multiplier. Moreover, $\|v\|^2 = \mathbb{E}_{\pi_k}[(\pi/\pi_k - 1)^2]$ is the Pearson χ^2 divergence.*

8.5 Positivity Safeguards

The closed-form linear response $v^*(y) = (\omega_\alpha(y) - 1)/\mu$ is derived in the tangent space of the probability manifold at π_k , and only guarantees first-order stationarity of the proximal objective. It does *not* enforce $\pi_k(y)(1 + v^*(y)) \geq 0$ outside a local neighborhood. When $\omega_\alpha(y) \ll 1$ and μ is small, one may have $v^*(y) < -1$, violating positivity.

Proposition 8.4 (Local Positivity Condition). *The update $\pi_{k+1} = \pi_k(1 + v^*)$ is a valid probability distribution whenever $\mu \geq \|\omega_\alpha\|_\infty - 1$, since then $v^*(y) = (\omega_\alpha(y) - 1)/\mu \geq -1$ for all y .*

In practice, positivity is maintained by one or more of: (i) choosing μ large enough relative to the escort weight range; (ii) clipping v^* to $[-1 + \epsilon, +\infty)$; (iii) projecting onto the probability simplex after the update. This is consistent with standard trust-region Taylor approximations in policy optimization and does not alter local convergence properties (Corollary 8.2).

9 Experiments

We conduct an empirical comparison of OPO against three strong baselines—GRPO, GSPO, and DAPO—on mathematical reasoning tasks using the VERL framework.

9.1 Experimental Setup

Model and Data. We use Qwen3-1.7B as the base model and train on MATH Level 3 problems. All methods use identical training configurations: 4 epochs, batch size 32, learning rate 2×10^{-6} , and 6 rollout generations per prompt.

Baseline Configurations.

- **GRPO** (Group Relative Policy Optimization) [4]: Standard token-level policy gradient with group-normalized advantages. Uses vanilla PPO loss mode without a value function critic.
- **GSPO** (Group Sequence Policy Optimization) [21]: Applies sequence-level importance ratios rather than token-level ratios, aiming for more granular credit assignment at the trajectory level.
- **DAPO** (Decoupled Clip and Dynamic sAmpling Policy Optimization) [20]: An advanced baseline incorporating four key mechanisms:
 1. **Clip Higher**: Raises the PPO clip upper bound (e.g., $1 + \epsilon \rightarrow 1.28$) to mitigate entropy collapse and preserve exploration.
 2. **Dynamic Sampling**: dynamically filters “all-correct” or “all-wrong” samples that contribute zero advantage, focusing training on informative samples.
 3. **Token-Level Policy Gradient**: Standardizes advantage weights across tokens in a mini-batch to prevent gradient dilution in long sequences.
 4. **Overlong Reward Shaping**: Applies a length-aware penalty and masks gradients for truncated responses to reduce noise.
- **OPO**: The proposed method with $\alpha = 0.4$, $\mu = 1.0$, on-policy anchoring ($\pi_{\text{ref}} = \pi_{\text{old}}$), and adaptive τ with range $[0.2, 1.5]$. Note: $1 - \alpha = 0.6$ controls the effective advantage amplification in Eq. (7).

9.2 Results

Overall Performance. Table 1 summarizes the key metrics across all four algorithms.

Table 1: Comparison of alignment algorithms on Qwen3-1.7B + MATH Level 3. Reward and gradient norm are averaged over the final 20 training steps. Higher gradient norm at convergence, combined with stable (non-exploding) training dynamics, indicates absence of gradient saturation rather than optimization instability.

Algorithm	Mean Reward	Grad Norm	Characteristics
GRPO	0.686	0.61	Standard baseline, stable
GSPO	0.713	0.50	Strong, some gradient decay
DAPO	0.67*	0.22	Conservative, early plateau
OPO (Ours)	0.756	0.90	Best reward, non-saturating gradients

Algorithm Characteristics.

- **GRPO:** Serves as the canonical baseline. Achieves reasonable performance (69% acc) with moderate gradient norms. The token-level normalization provides stability but may average out strong signals.
- **GSPO:** Improves upon GRPO (71% acc) via sentence-level credit assignment. However, gradient norms (0.50) are lower than OPO’s, suggesting some saturation in high-confidence regimes.
- **DAPO:** Exhibits the lowest gradient norms (0.22) and plateaus early. The conservative clipping constraints appear overly restrictive for reasoning tasks where continued learning is beneficial.
*Note: Reward fluctuated between 0.59–0.67.
- **OPO:** Achieves the highest mean reward (0.756) while maintaining the largest gradient norms (0.90). This empirically validates the theoretical prediction: the χ^2 geometry provides non-saturating linear gradients, allowing the model to continue learning where others plateau.

Training Dynamics. Figure 4 shows the training accuracy (mean reward) over 224 training steps.

- **Early Stage:** GRPO exhibits the fastest initial learning, surpassing OPO in the first 50 steps. This is consistent with standard policy gradient methods having aggressive early updates.
- **Late Stage Cross-over:** As training progresses (after step 100), GRPO and GSPO begin to saturate. In contrast, OPO maintains a steady improvement rate, eventually overtaking all baselines to reach the highest final accuracy (~76%). This confirms that the χ^2 -induced linear drive prevents the “vanishing gradient” problem common in KL-constrained methods as confidence increases.

Gradient Behavior. Figure 5 illustrates the gradient norm dynamics across training. OPO exhibits consistently higher but stable (non-exploding) gradient norms throughout training, validating the non-saturating property of the χ^2 geometry. The stability of these norms rules out the alternative explanation of optimization instability or under-regularization. DAPO shows severely diminished gradients, explaining its early plateau.

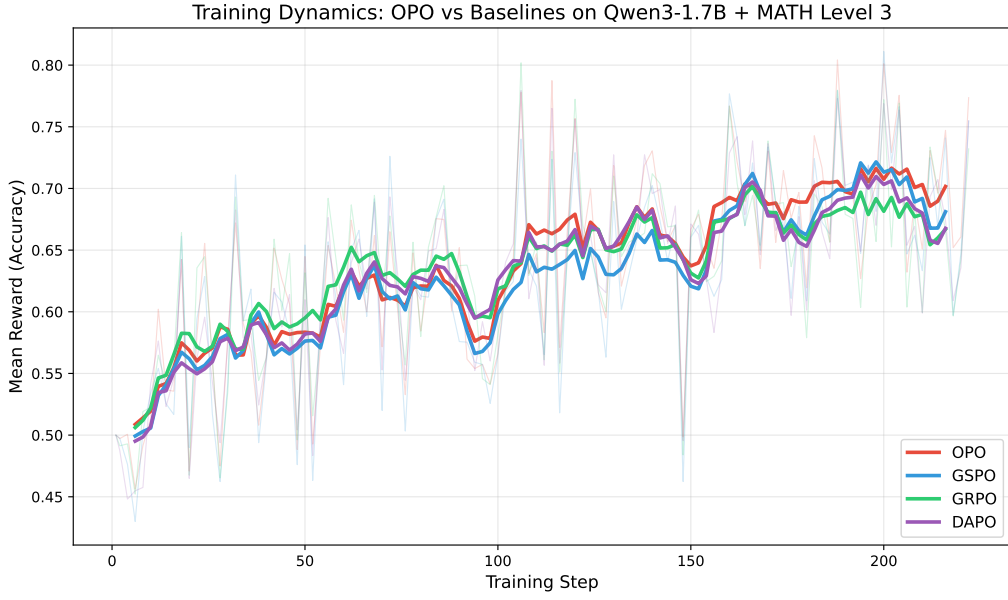


Figure 4: Training dynamics on Qwen3-1.7B Math RL. Note the cross-over behavior: GRPO (green) starts strong but plateaus, while OPO (red) sustains improvement and achieves the highest final performance.

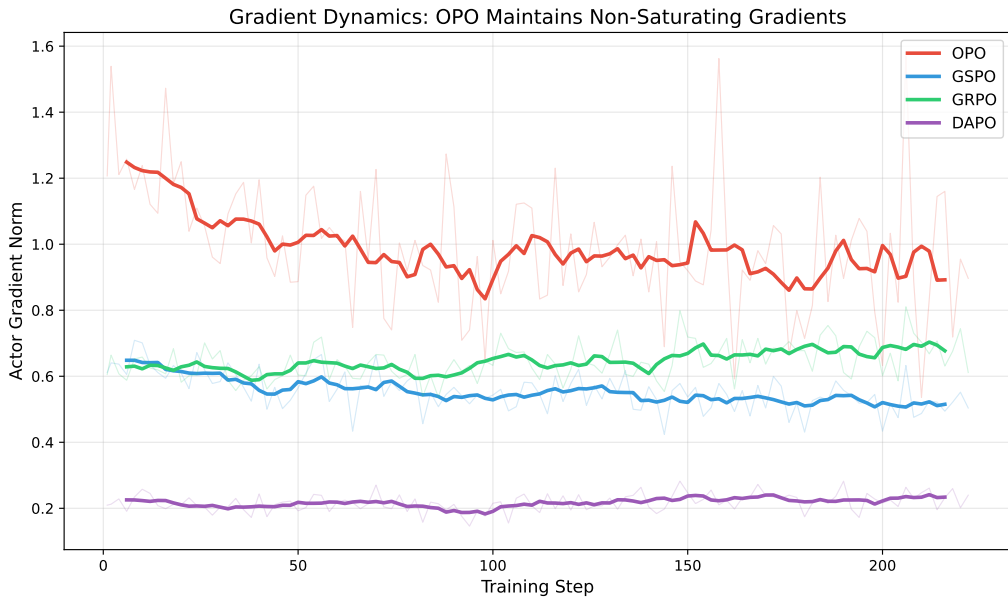


Figure 5: Gradient norm comparison. OPO maintains healthy gradient norms (0.9) throughout training, while DAPO (0.22) and GSPO (0.50) exhibit gradient decay.

Gradient Saturation Analysis. Figure 6 provides direct evidence for OPO’s non-saturating property. Panel (a) plots gradient norms against mean reward (a confidence proxy). As the model becomes more confident (higher reward), GRPO and GSPO gradients exhibit a decaying trend, and DAPO gradients remain near zero. In contrast, OPO maintains elevated gradient norms across all confidence levels.

Panel (b) addresses the fact that different methods operate at different advantage scales (e.g., GRPO z -scores advantages to $\sigma \approx 2$, whereas OPO uses raw advantages with $\sigma \approx 0.2$). To enable a fair comparison, we plot the *gradient response efficiency* $\|\nabla\| / (\frac{1}{2} \text{AdvRange})$ over training steps, normalizing gradient magnitude by the advantage signal amplitude. OPO sustains an efficiency of $\sim 1.0\text{--}1.5$ throughout training, approximately $5\times$ higher than GRPO ($\sim 0.2\text{--}0.3$) and DAPO (~ 0.1). This confirms the linear response prediction of Theorem 4.3: under χ^2 geometry, each unit of advantage signal produces a proportional gradient update, whereas KL-based objectives attenuate the signal through their policy-dependent curvature.

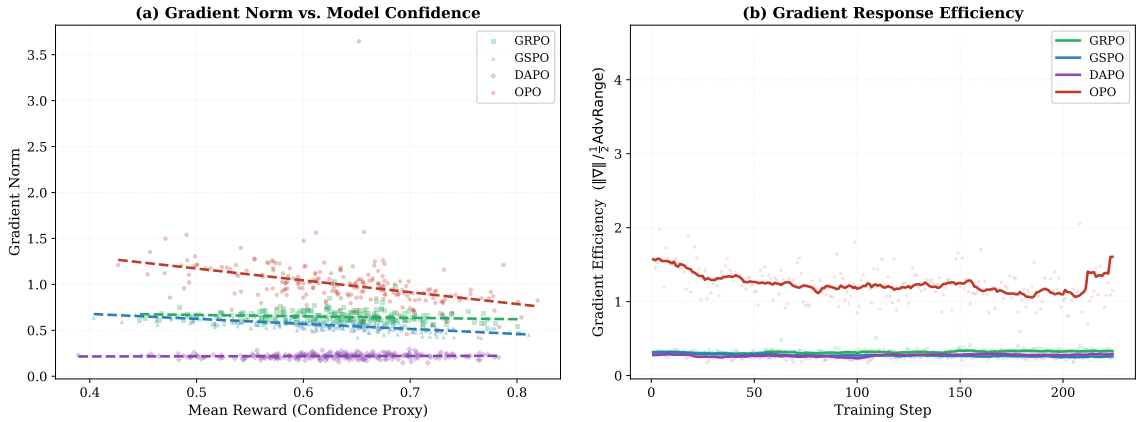


Figure 6: Gradient saturation analysis. (a) Gradient norm vs. mean reward (confidence proxy): OPO maintains non-saturating gradients as confidence grows, while baselines decay. (b) Gradient response efficiency (gradient norm normalized by advantage amplitude) over training: OPO sustains $\sim 5\times$ higher gradient-per-signal than baselines, confirming the constant-curvature prediction of χ^2 geometry.

Entropy Dynamics. Figure 7 depicts the policy entropy throughout training. OPO maintains consistently higher entropy levels compared to baselines. We attribute this to the granularity of supervision: GRPO and DAPO utilize **token-level** updates, imposing dense supervision that forces the policy to collapse rapidly into specific phrasings. In contrast, OPO (and GSPO) employs **sequence-level** updates, where y denotes an entire response trajectory and the loss is averaged over complete sequences rather than individual tokens. This “sparse” supervision aligns the total trajectory probability without micromanaging individual tokens, thereby preserving policy diversity and exploration potential.

Summary of Findings. The experimental results confirm that OPO’s orthogonalized design—combining α -weighted sampling with χ^2 optimization geometry—prevents gradient saturation and enables continued learning in high-confidence regimes. The gradient saturation analysis (Figure 6) provides the most direct evidence: OPO’s gradient magnitude remains proportional to advantage amplitude (linear response), while KL-based baselines exhibit suppressed gradients regardless of the driving signal.

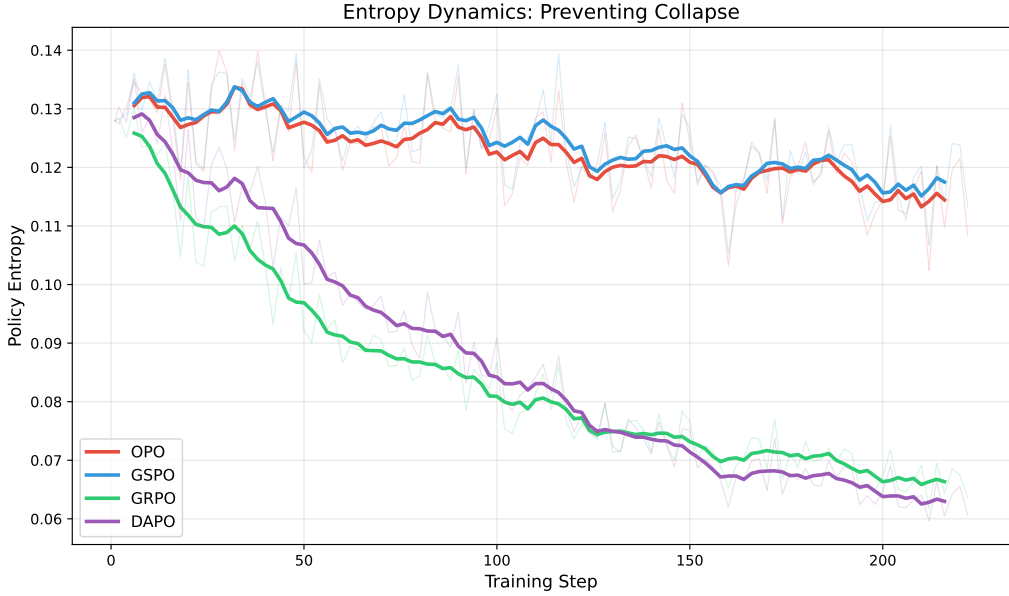


Figure 7: Entropy dynamics. OPO maintains higher entropy than baselines, preventing premature mode collapse and enabling sustained exploration throughout the training process.

10 Discussion

Relation to Existing Methods. OPO can be viewed as occupying a previously unexplored point in the design space:

- $\alpha \rightarrow 1$ (conservative escort): $\omega_\alpha \rightarrow 1$, recovering supervised fine-tuning–like uniform weighting.
- $\alpha \rightarrow 0$ (aggressive escort) with KL geometry: the exponential-type weighting resembles KL-regularized preference optimization (e.g., DPO), but inherits gradient saturation.
- **OPO**: moderate α (peak-seeking escort) *combined with* Euclidean (χ^2) geometry—non-saturating gradients with advantage-aware sampling.

Geometry Comparison. Table 2 summarizes the structural differences among representative methods.

Table 2: Comparison of sampling and optimization geometries across alignment methods.

Method	Sampling Geometry	Optimization Geometry
PPO / GRPO	implicit KL	KL curvature (ratio clip)
DPO	KL	KL curvature (sigmoid)
OPO (Ours)	α -escort (tunable)	χ^2 curvature (constant μI)

Geometric Interpretation of Entropy Preservation. From a geometric perspective, KL geometry inherits a logarithmic penalty on low-probability outcomes: $-\log \pi(y)$ diverges as $\pi(y) \rightarrow 0$, strongly suppressing entropy by penalizing any residual mass on unlikely tokens. In contrast, χ^2 geometry penalizes deviations quadratically in ratio space: the cost $(\pi/\pi_k - 1)^2$ remains finite even when $\pi(y) \ll \pi_k(y)$, which attenuates the shrinkage of low-probability mass and thus helps maintain entropy. This geometric explanation complements the sequence-level vs. token-level distinction discussed in the experiments.

Computational Cost. OPO incurs no additional model forward/backward passes compared to DPO/GRPO; the extra bookkeeping for ω_α is lightweight in practice.

Role of the Reference Policy. In OPO, the reference policy π_{ref} serves solely as an *origin* defining the coordinate system for the ratio $v_\theta = \pi_\theta / \pi_{\text{ref}} - 1$, rather than as an explicit regularizer via KL divergence. Stability is instead enforced by the quadratic penalty $\frac{\mu}{2}v^2$. This decoupling clarifies the distinct roles of anchoring (coordinate system) and regularization (optimization geometry).

Implementation Notes. The OPO objective (Equation (9)) involves expectations under π_{ref} . In practice:

- For on-policy training where samples come from $\pi_{\text{ref}} = \pi_{\text{old}}$, the batch itself provides an unbiased estimate.
- **Mini-batch anchoring.** Within one outer iteration, π_{ref} is frozen at the policy snapshot taken *before* the first mini-batch gradient step. All subsequent mini-batches in the same iteration share this anchor, ensuring that the log-ratio $\Delta_\theta = \log \pi_\theta - \log \pi_{\text{ref}}$ is evaluated against a consistent reference. This is analogous to PPO’s “epoch” convention and guarantees that Δ_θ starts near zero at the beginning of each outer iteration, supporting the local linear approximation $v \approx \Delta$.
- For off-policy settings, importance sampling or a separate reference sample set can be used.

Limitations. The framework introduces hyperparameters (α, μ) that may require tuning. Our experiments focus on reasoning tasks; validation on diverse domains (code generation, general instruction following) remains future work. Larger-scale experiments across diverse tasks and model sizes are needed to fully characterize the strengths and limitations of OPO.

11 Conclusion

We have presented **Orthogonalized Policy Optimization (OPO)**, grounded in a unified work–dissipation principle: the policy update maximizes external work from an α -escort sampling field while paying a quadratic dissipation cost in χ^2 ratio geometry. This single variational principle admits three equivalent interpretations—mirror descent, Hilbert-space projection, and linear response—confirming that OPO is the canonical quadratic proximal response in ratio geometry. The resulting framework has constant Hessian, linear non-saturating gradients, global contraction, and reveals advantage z -scoring as a conservation-law projection. Experiments on mathematical reasoning tasks validate that OPO outperforms KL-based methods where gradient saturation limits further improvement.

References

- [1] R. Rafailov, A. Sharma, E. Mitchell, S. Ermon, C. D. Manning, and C. Finn. Direct Preference Optimization: Your Language Model is Secretly a Reward Model. *NeurIPS*, 2023.
- [2] J. Schulman, F. Wolski, P. Dhariwal, A. Radford, and O. Klimov. Proximal Policy Optimization Algorithms. arXiv:1707.06347, 2017.
- [3] J. Schulman, S. Levine, P. Moritz, M. I. Jordan, and P. Abbeel. Trust Region Policy Optimization. *ICML*, 2015.
- [4] Z. Shao, P. Wang, Q. Zhu, R. Xu, J. Song, X. Bi, H. Zhang, M. Zhang, Y. K. Li, Y. Wu, and D. Guo. DeepSeekMath: Pushing the Limits of Mathematical Reasoning in Open Language Models. arXiv:2402.03300, 2024.
- [5] P. Christiano, J. Leike, T. B. Brown, M. Martic, S. Legg, and D. Amodei. Deep Reinforcement Learning from Human Preferences. *NeurIPS*, 2017.
- [6] L. Ouyang, J. Wu, X. Jiang, D. Almeida, C. L. Wainwright, P. Mishkin, et al. Training Language Models to Follow Instructions with Human Feedback. *NeurIPS*, 2022.

- [7] M. G. Azar, M. Rowland, B. Piot, D. Guo, D. Calandriello, M. Valko, and R. Munos. A General Theoretical Paradigm to Understand Learning from Human Preferences. *AISTATS*, 2024.
- [8] Y. Meng, M. Xia, and D. Chen. SimPO: Simple Preference Optimization with a Reference-Free Reward. *NeurIPS*, 2024.
- [9] I. Csiszár. Information-type measures of difference of probability distributions and indirect observations. *Studia Sci. Math. Hungar.*, 2:299–318, 1967.
- [10] S. M. Ali and S. D. Silvey. A General Class of Coefficients of Divergence of One Distribution from Another. *JRSS-B*, 28(1):131–142, 1966.
- [11] S. Amari. *Information Geometry and Its Applications*. Springer, 2016.
- [12] Y. Li and R. E. Turner. Rényi Divergence Variational Inference. *NeurIPS*, 2016.
- [13] S. Nowozin, B. Cseke, and R. Tomioka. f-GAN: Training Generative Neural Samplers Using Variational Divergence Minimization. *NeurIPS*, 2016.
- [14] S. K. S. Ghasemipour, R. Zemel, and S. Gu. A Divergence Minimization Perspective on Imitation Learning Methods. *CoRL*, 2020.
- [15] H. Xu *et al.* Improving Proximal Policy Optimization with Alpha Divergence. *Neurocomputing*, 2023.
- [16] Z. Wang. APO: Alpha-Divergence Preference Optimization. arXiv:2512.22953, 2025.
- [17] Z. Wang. ADPO: Anchored Direct Preference Optimization. arXiv:2510.18913, 2025.
- [18] R. Kubo. The fluctuation-dissipation theorem. *Rep. Prog. Phys.*, 29(1):255–284, 1966.
- [19] L. D. Landau, E. M. Lifshitz, and L. P. Pitaevskii. *Statistical Physics, Part 1*. Pergamon Press, 3rd edition, 1980.
- [20] Q. Yu, Z. Zhang, R. Zhu, Y. Yuan, X. Zuo, Y. Yue, W. Dai, T. Fan, G. Liu, and L. Liu. DAPO: An Open-Source LLM Reinforcement Learning System at Scale. arXiv:2503.14476, 2025.
- [21] C. Zheng, S. Liu, M. Li, X. Chen, B. Yu, C. Gao, K. Dang, Y. Liu, R. Men, A. Yang, J. Zhou, and J. Lin. Group Sequence Policy Optimization. arXiv:2507.18071, 2025.

A Theoretical Proofs and Derivations

A.1 Log-Ratio Approximation Error

Lemma A.1 (Log-Ratio Approximation Error). *Let $\Delta_\theta(y) = \log \pi_\theta(y) - \log \pi_{\text{ref}}(y)$ be the log-ratio, and $v_\theta(y) = \exp(\Delta_\theta(y)) - 1$ be the exact ratio deviation. Let $\delta = \|\Delta_\theta\|_\infty$. For sufficiently small δ (in particular $\delta < 1$, which holds under the small trust-region regime maintained by on-policy anchoring and the χ^2 penalty $\frac{\mu}{2}\mathbb{E}[v^2]$):*

$$|v_\theta - \Delta_\theta| \leq \frac{1}{2}\delta^2 e^\delta, \quad |v_\theta^2 - \Delta_\theta^2| \leq \delta^3 e^{2\delta} \quad (21)$$

Consequently, the difference between the exact ratio loss and the log-approximate loss scales as $O(\mathbb{E}[\Delta_\theta^3])$.

Proof. Using Taylor expansion $e^x = 1 + x + \frac{x^2}{2} + \dots$, we have $v = \Delta + \frac{\Delta^2}{2} + O(\Delta^3)$. The bounds follow from standard remainder estimation for the exponential function.

A.2 Equivalence to χ^2 -Constrained Maximization

Proposition A.2 (Lagrange Dual Equivalence). *Consider the problem of maximizing alignment with the target ω_α subject to a functional χ^2 trust region:*

$$\max_{v \in L^2(\pi_{\text{ref}})} \mathbb{E}_{\pi_{\text{ref}}} [\omega_\alpha(y)v(y)] \quad \text{s.t.} \quad \mathbb{E}_{\pi_{\text{ref}}} [v(y)^2] \leq \epsilon \quad (22)$$

The Lagrangian relaxation of this problem is exactly the OPO objective $\mathcal{L}_{\text{OPO}} = -\mathbb{E}[\omega_\alpha v] + \frac{\mu}{2}\mathbb{E}[v^2]$, where the regularization coefficient μ is the Lagrange multiplier corresponding to the trust region radius ϵ .

The optimal solution is $v^*(y) = \frac{1}{\mu}\omega_\alpha(y)$. This duality implies that α purely shapes the objective (alignment direction), while μ purely enforces the feasibility radius (optimization geometry).

A.3 Proof of Proposition 4.2: α -Geometric Interpolation

Proof. Define the oracle target $P^*(y) \propto \exp(A(y))$ and the parameterized family $\rho_\alpha(y) \propto \tilde{p}(y)^\alpha P^*(y)^{1-\alpha}$ for $\alpha \in [0, 1]$.

Step 1 (Geodesic structure). In the e -affine coordinate system of the statistical manifold [11], the log-density of ρ_α is:

$$\log \rho_\alpha(y) = \alpha \log \tilde{p}(y) + (1 - \alpha) \log P^*(y) - \log Z_\alpha \quad (23)$$

where Z_α is the normalizing constant. Since $\log \rho_\alpha$ is an affine function of α in the natural parameter, $\{\rho_\alpha\}_{\alpha \in [0, 1]}$ forms an e -geodesic (exponential geodesic) connecting P^* (at $\alpha = 0$) to \tilde{p} (at $\alpha = 1$) in the exponential family.

Step 2 (Importance weight). The sampling weight is:

$$\omega_\alpha(y) = \frac{\rho_\alpha(y)}{\tilde{p}(y)} \propto \left(\frac{P^*(y)}{\tilde{p}(y)} \right)^{1-\alpha} \quad (24)$$

In the on-policy setting where $P^*(y) = \exp(A(y))$ and $\tilde{p} = \pi_{\text{old}}$, this yields $\omega_\alpha \propto (\exp(A)/\tilde{p})^{1-\alpha}$, which simplifies to $\exp((1-\alpha)A)$ when the \tilde{p} correction is absorbed by the sampling measure.

Step 3 (Geometric consistency). This interpolation corresponds to the exponential geodesic in the statistical manifold and is consistent with Rényi α -divergence interpolation geometry [11]. Under the dually flat structure of exponential families, it coincides with the e -projection onto the geodesic submanifold connecting \tilde{p} and P^* .

A.4 Distributional Stability Guarantees

Proposition A.3 (χ^2 Controls Total Variation). *Let $TV(\pi, \pi_{\text{ref}}) = \frac{1}{2}\mathbb{E}_{\pi_{\text{ref}}} [|i(y) - 1|] = \frac{1}{2}\mathbb{E}[|v(y)|]$. By Jensen's inequality:*

$$TV(\pi, \pi_{\text{ref}}) = \frac{1}{2}\mathbb{E}[|v|] \leq \frac{1}{2}\sqrt{\mathbb{E}[v^2]} \quad (25)$$

Thus, bounding the χ^2 norm $\mathbb{E}[v^2] \leq \epsilon$ guarantees that the policy remains within a $\sqrt{\epsilon}/2$ -radius of the reference in Total Variation distance.